Geomechanics and Engineering, *Vol. 15, No. 5 (2018) 1113-1124*
DOI: https://doi.org/10.12989/gae.2018.15.5.1113

Strength and failure characteristics of the rock-coal combined body with single joint in coal

Da W. Yin[1,2a], Shao J. Chen[*1,2], Bing Chen[1b], Xing Q. Liu[1b] and Hong F. Ma[1b]

[1]*College of Mining and Safety Engineering, Shandong University of Science and Technology, 579 Qianwanggang Road, Huangdao District, Qingdao, Shandong Province, 266590, China*
[2]*Key Laboratory of Safety and High-efficiency Coal Mining, Ministry of Education, Anhui University of Science and Technology, Huainan 232001, China*

(Received April 29, 2017, Revised January 4, 2018, Accepted January 14, 2018)

Abstract. Geological dynamic hazards during deep coal mining are caused by the failure of a composite system consisting of the rock and coal layers, whereas the joint in coal affects the stability of the composite system. In this paper, the compression test simulations for the rock-coal combined body with single joint in coal were conducted using PFC^{2D} software and especially the effects of joint length and joint angle on strength and failure characteristics in a rock-coal combined body were analyzed. The joint length and joint angle exhibit a deterioration effect on the strength and affect the failure modes. The deterioration effect of joint length of L on the strength can be neglected with a tiny variation at α of 0° or 90° between the loading direction and joint direction. While, the deterioration effect of L on strength are relatively large at α between 30° and 60°. And the peak stress and peak strain decrease with the increase of L. Additionally, the deterioration effect of α on the strength becomes larger with the increase of L. With the increase of α, the peak stress and peak strain first decrease and then increase, presenting "V-shaped" curves. And the peak stress and peak strain at α of 45° are the smallest. Moreover, the failure mainly occurs within the coal and no apparent failure is observed for rock. At α between 30° and 60°, the secondary shear cracks generated in or close to the joint tips, cause the structural instability failure of the combined body. Therefore, their failure models present as a shear failure along partial joint plane direction and partially cutting across the coal body or a shear failure along the joint plane direction. However, at α of 60° and L of 10 mm, the "V-shaped" shear cracks cutting across the coal body cause its final failure. While crack nucleations at α of 0° or 90° are randomly distributed in the coal, the failure mode shows a V-shaped shear failure cutting across the coal body.

Keywords: particle flow simulation; strength and failure characteristics; rock-coal combined body; single joint in coal; joint length and joint angle

1. Introduction

In the process of deep coal mining, geological dynamic hazards frequently occur in many coal mines, such as rock bursts, coal bumps, gas outburst and floor heaves, causing potential safety hazards for coal production safety. Meanwhile, the geological dynamics hazards in coal mining are caused by the failure of a composite system consisting of rock and coal layers (Zhao *et al.* 2016, Lu *et al.* 2015, Chen *et al.* 2016, 2017). Therefore, it is of great significance to study the strength and failure characteristics of the rock-coal combined body for preventing dynamic geological hazards and ensuring the safety production in the deep coal mining engineering.

A lot of studies have been conducted on the strength and failure characteristics of the rock-coal combined body by many domestic and foreign scholars. Petukhov and Linkov (1979) analyzed the stability of general bipartite system and rock-coal system while studying the stable behavior of rock mass after post-peak point. Based on the Coulomb-Mohr yield criterion, a failure criterion for composite rocks materials was established and discussed (Landriani and Taliercio 1998). The effects of rock strength on the mechanical behavior and failure mode of a coal-rock combined body were studied (Liu *et al.* 2015). The strength and failure characteristics of a rock-coal combined body with a height ratio of 1:1 under the cyclic loading and unloading condition were studied by Zuo *et al.* (2011). Four different types of three-body model composed of rock and coal with different strength and stiffness were established and the failure characteristics of compound model such as roof-coal-floor were studied (Zhao *et al.* 2014). A series of uniaxial and triaxial creep tests on shale specimens in coal measure were carried out for investing the deformation characteristics of roof rock with regards to time and failure mechanism under complex stress conditions (Mishra and Verma 2015). The effects of loading and unloading rate on the deformation and failure behaviors of the composite rock and coal layers were studied (Huang and Liu 2013). The influences of the interfacial angle on the rock-coal combined body were investigated with experimental and numerical method (Zhao *et al.* 2016).

∗Corresponding author, Professor
E-mail: chensj@sdust.edu.cn
[a]Ph.D.
[b]Master Student

ISSN: 2005-307X (Print), 2092-6219 (Online)

The above achievements have great important significance for understanding of the strength and failure characteristics of the rock-coal combined body. However, these studies are all focused on the intact rock-coal combined body. Meanwhile, rock and coal are natural materials formed by the aggregation of mineral particles and cement with a determinate rule under the long-term geological effects. Generally, rock is relatively dense and it has almost no macroscopic native defects. While, raw coal is relatively soft and there is a significant amount of native defects in it. Among them, the joint is a common native defect, playing an important role in the stability of the rock-coal combined body in practical coal mining engineerings. And the researches of the effect of joint characteristics on the strength and failure characteristics are more focused on the single rock, coal or rock-like specimens (Zhao *et al.* 2015, Cao *et al.* 2016, Liang *et al.* 2012, Yang 2015). There are few studies on the effects of the joint characteristics on the strength and failure characteristics on the rock-coal combined body. Yin *et al.* (2018) studied and analyzed the effects of joint angle in coal on the strength, acoustic emission (AE) and failure characteristics of a roof rock-coal combined body using PFC^{2D} software.

The particle flow code (PFC) is an effective method to study the macro-mechanics problems at the micro-level. And it can essentially reveal the deformations and failure regimes of coal and rock, which has been widely applied in uniaxial compression test simulations, biaxial compression test simulations and triaxial compression test simulations (Lee and Jeon 2011, Zhao *et al.* 2016, Yin *et al*. 2018, Zhao *et al*. 2015).

In this paper, the compression test simulations of the rock-coal combined body with single joint in coal were conducted using PFC^{2D} software and the purpose was to interpret the effecting mechanism of joint characteristics (joint length and joint angle) on the strength and failure characteristics of the rock-coal combined body. The aforementioned achievements can improve the comprehension of the strength and failure characteristics of the rock-coal combined body with single joint in coal.

2. Numerical model and simulation test conditions

2.1 Micro-parameters of rock and coal

In PFC, the parallel bond model refers to plane-to-plane bond and the moment of force can be transmitted. Therefore, it is applied to simulating the compact material, such as rock and coal (Manouchehrian *et al*. 2014). In this study, the compression model for the rock-coal combined body with single joint in coal was built using the parallel bond model.

In the parallel bond model, the macroscopic mechanical properties of the rock and coal are mainly affected by the micro-parameters of particles in PFC^{2D} software, i.e., contact modulus of the particle, parallel bond elastic modulus, parallel bond normal strength, parallel bond tangential strength, etc. The determination of micro-parameters of rock and coal is the process of minimizing the error between simulation results and experimental results by adjusting the micro-parameters based on the elastic modulus, Poisson's ratio, peak stress of the standard specimen (ϕ 50 mm×100 mm) achieved by the laboratory test. Due to the limitation of laboratory test condition, the micro-parameters of rock and coal provided by Zhang *et al.* (2016) and Yin *et al.* (2018) were used to carry out numerical test, as shown in Table 1.

Table 1 Micro-parameters of rock and coal (Zhao *et al.* 2016, Yin *et al*. 2018)

Parameters	Rock	Coal	Parameters	Rock	Coal
Minimum particle size/mm	0.2		Parallel bond elastic modulus /GPa	12	4
Particle size ratio	1.5		Parallel bond normal strength /MPa	45	15
Density/kg/m^3	2600	1800	Parallel bond tangential strength/MPa	45	15
Contact modulus of the particle /GPa	12	4	Parallel bond normal stiffnes/ tangential stiffnes	2.5	
Parallel bond radius multiplier	1		Normal stiffnes/tangential stiffnes	2.5	
Coefficient of friction	0.5				

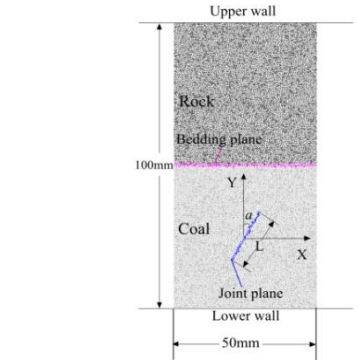

(a) PFC^{2D} model

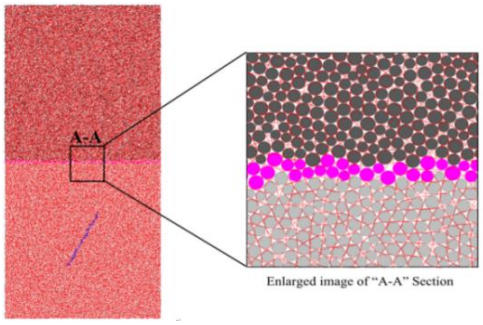

(b) Schematic diagram of parallel bond

Fig. 1 PFC^{2D} model of the rock-coal combined body with single joint in coal

2.2 PFC^{2D} model construction

Particle flow model of the rock-coal combined body with single joint in coal was established and generated by the radius extension, as shown in Fig. 1. In Fig. 1, the parallel bond is represented in red lines. The model size is ϕ 50 mm ×100 mm. In this model, the minimum particle radius is 0.2 mm, and the maximum radius is 0.3 mm. The height ratio of rock to coal is taken as 1:1. And a total of 21390 particles were generated in the model. The bedding plane and joint plane were generated by the JSET

Table 2 Simulation test conditions

Conditions	α/°	L/mm	Conditions	α/°	L/mm
1	0	10	11	45	30
2	0	20	12	45	40
3	0	30	13	60	10
5	30	10	15	60	30
6	30	20	16	60	40
7	30	30	17	90	10
8	30	40	18	90	20
9	45	10	19	90	30
10	45	20	20	90	40

command. For facilitating the distinction, the particles through the bedding plane are represented by a magenta color and the particles through the joint plane represented in blue.

Based on various researches, the micro-parameters of the bedding plane and joint planeare set to very small values (Zhao *et al*. 2015, Kulatilake *et al.* 2001, Park and Song 2009, Yin *et al*. 2018). In this study, the micro-parameters of bedding plane were taken same as that of joint plane. Therefore, the friction coefficient was set as 0.1, parallel bond normal strength and parallel bond tangential strength were set as 0 MPa and parallel normal stiffnes and parallel bond tangential stiffnes taken as 0 N/m.

Now, the rock-coal combined body model with single joint in coal has been built. The unbalanced force generated in this process was eliminated cyclically. The wall was lengthened appropriately for preventing the spill-out of particles. For this work to be executed, the loading is performed by moving the upper and lower walls at a loading rate of 0.1 m/s. And the loading is terminated when the axial stress is 10% of the peak stress.

2.3 Simulation test conditions

In order to study the effecting mechanism of joint length and joint angle on strength and failure characteristics of the rock-coal combined body, the length of L were taken as 10 mm, 20 mm, 30 mm and 40 mm, and the included angle of α between the single joint and loading direction taken as 0°, 30°, 45°, 60° and 90°. The L and α were combined with each other and there are 20 test simulation conditions, as shown in Table 2.

3. Strength characteristics of the rock-coal combined body with single joint in coal

3.1 Effects of joint length and joint angle on the stress-strain behavior

For contrastively analyzing the effects of joint length and joint angle on the stress-strain behaviour of the rock-coal combined body, Fig. 2 illustrates the stress-strain curves of single rock sample, single coal sample, intcat rock-coal combined body and combined bodies with single

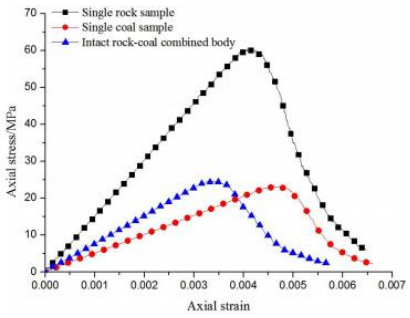

(a) Single rock, coal samples and intact combined body

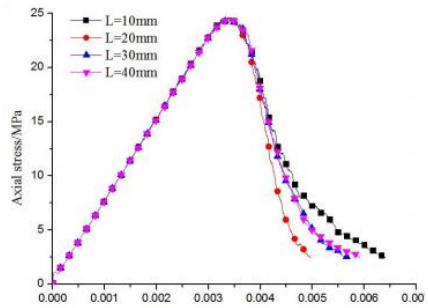

(b) α=0°

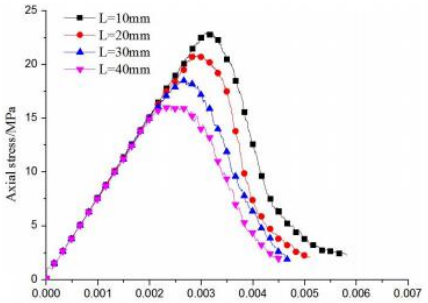

(c) α=30°

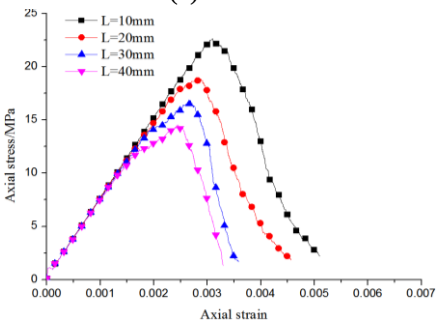

(d) α=45°

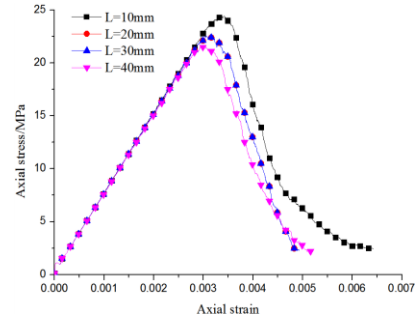

(e) α=60°

Fig. 2 Uniaxial compressive stress-strain curves of single rock sample, single coal sample, intcat rock-coal combined body and combined bodies with single joint in coal under different conditions of α

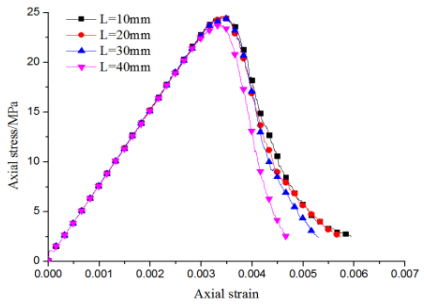

(f) α=90°

Fig. 2 Continued

Table 3 Simulation test results

Conditions	Peak stress/MPa	Peak strain/%	Conditions	Peak stress/MPa	Peak strain/%
Single rock sample	60.346	0.416	10	18.821	0.287
Single coal sample	23.182	0.459	11	16.759	0.268
Intact rock-coal combined body	24.664	0.346	12	14.536	0.235
1	24.586	0.344	13	24.404	0.342
2	24.633	0.342	14	22.882	0.314
3	24.625	0.341	15	22.701	0.314
4	24.534	0.344	16	21.612	0.297
5	22.992	0.319	17	24.633	0.339
6	20.952	0.286	18	24.612	0.343
7	18.523	0.266	19	24.449	0.341
8	16.209	0.239	20	23.768	0.333
9	22.617	0.310		—	

joint in coal under different conditions of α and Fig. 3 presents the stress-strain curves of rock-coal combined bodies under different conditions of L. Also, the simulaition test results are given in Table 3.

In Figs. 2 and 3, the stress-strain curves of single rock sample, single coal sample, intcat rock-coal combined body and combined bodies are quite similar, which can be divided into four stages, ranging from linear elastic deformation stage, non-linear deformation stage, post-peak strain softening and residual strength stage. In Fig. 2(a), the stress-strain curve of the intact combined body is located between the curves of single rock and coal samples, and close to the single coal sample curve, which is similar to the research results studied by Liu *et al.* (2015). And the elastic modulus of intact combined body is larger than that of single coal sample, but less than that of single rock sample. While, there is no obvious change for the elastic modulus of combined bodies with single joint in coal, indicating that the stress-strain curves are coincident at the linear elastic deformation stage. The L and α do not affect the compression failure process of the rock-coal combined body, but affect the strain required for each stage and have deterioration effects on the strength. In Table 3, the peak stress of single rock sample is the largest. And when α is 0° or 90°, no matter what the value of L is, the peak stresses of combined bodies with single joint in coal are close to that of the intact combined body and larger than that of single coal sample. Moreover, when α is between 30° and 60°, the peak stresses of combined bodies with single joint in coal are generally less than that of intact combined body and single

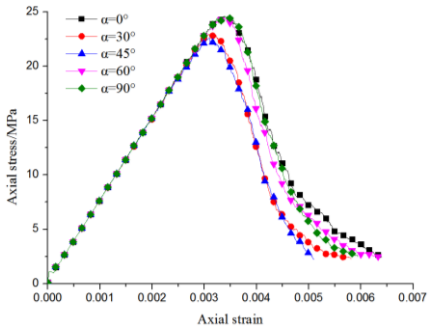

(a) L=10 mm

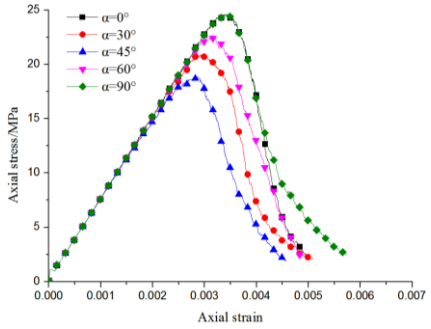

(b) L=20 mm

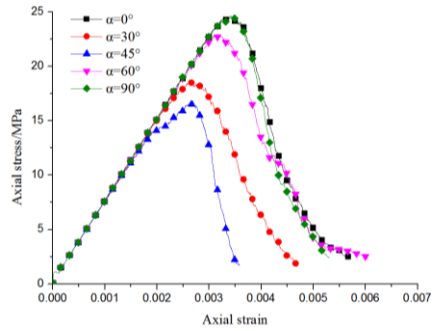

(c) L=30 mm

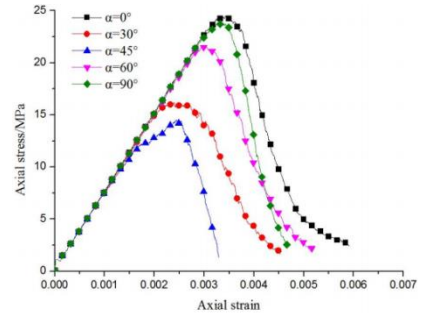

(d) L=40 mm

Fig. 3 Uniaxial compressive stress-strain curves of combined bodies with single joint under different conditions of L

coal sample. The above analysis show that due to the differences of joint lengths and joint angles, the deterioration effects on strength of the combined body are not necessarily same. Thus, the effects of joint length and joint angle on strength characteristics were analyzed as following.

3.2 Effects of the joint length and joint angle on strength characteristics

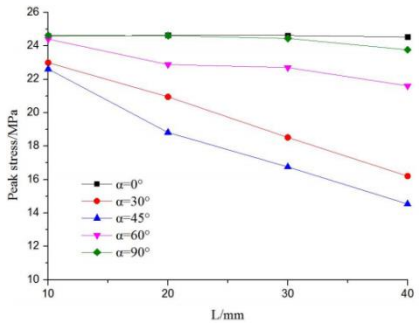

(a) Relationship between the peak stress and L

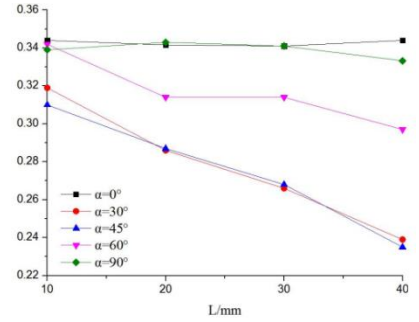

(b) Relationship between the peak strain and L

Fig. 4 Variation trend of peak stress and peak strain with the change of L

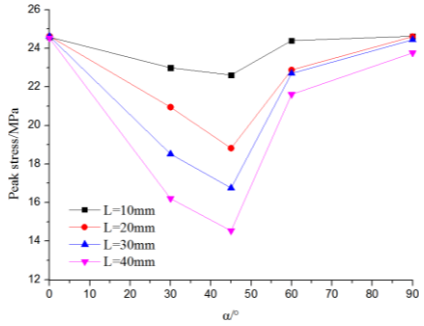

(a) Relationship between the peak stress and α

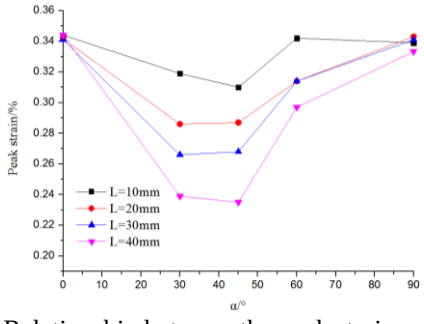

(b) Relationship between the peak strain and α

Fig. 5 Variation trend of the peak stress and peak strain with the change of α

Fig. 4 shows the variation trend of peak stress and peak strain with the change of L. In Figs. 2 and 4, when α is between 30° and 60°, the deterioration effect of L on the strength is relatively large, especially at α of 45°. With the increase of L, the peak stress and peak strain decrease. As an example, when α is 45°, compared with the joint length of 10 mm, peak stresses at L of 20 mm, 30 mm and 40 mm decrease by 16.378%, 25.309% and 35.723%, respectively.

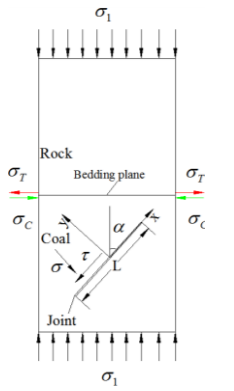

(a)

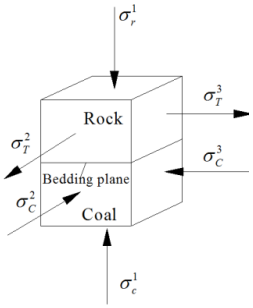

(b)

Fig. 6 Illustration of stress state distribution feature and three-dimension unit cell representative model of rock-coal combined body

And peak strains decrease by 7.419%, 13.548% and 24.194%, respectively. While, when α is 0° or 90°, the deterioration effect of L on the strength is relatively lower, which may be neglected. With the increase of L, the peak stress and peak strain have fluctuated with a tiny variation.

Fig. 5 shows the variation trend of peak stress and peak strain with the change of α under the same conditions of L. In Figs. 3 and 5, the deterioration effects of α on the strength becomes larger with the increase of L. Under a same condition of L, the peak stress and peak strain first decrease and then increase with the increase of α, presenting a "V-shaped" curve. When α is 45°, the peak stress and peak strain are the smallest.

A mechanical model was built firstly for the rock-coal combined body with single joint in coal, as shown in Fig. 6 (a). Meanwhile, the mechanical model satisfies the following assumptions: 1) Rock and coal are isotropic homogeneous bodies; 2) The strengths of rock, coal and joint plane are governed by the Coulomb-Mohr yield criterion. In Fig. 6 (a), σ_1 is the axial stress, τ and σ are the shear stress and normal stress on the joint plane, respectively. The elastic moduli of rock and coal are E_r and E_c, and Poisson ratios are u_S and u_C, respectively. And $E_r > E_c$, $u_r < u_c$. In order to maintain the consistent lateral deformation at the rock-coal bedding plane under the axial stress, the lateral deformation of coal near the bedding plane is limited in a certain extent by rock and the compressive stress of σ_C for coal is derived near the bedding plane. While, the lateral deformation of rock near the bedding plane is enhanced in a certain extent by the coal and a tensile stress of σ_T for rock is derived near the bedding plane. Due to the variation of the stress distribution near the

bedding plane, a three-dimensional representative model considering the zones near the bedding plane are taken for analyzing the strength of rock-coal combined body, as shown in Fig. 6(b). Among them, σ^3_T and σ^2_T are tensile stresses for rock in two horizontal directions, respectively. And σ^3_C and σ^2_C are compressive stresses for coal in two horizontal directions, respectively. σ^1_r and σ^1_c denote the axial stresses for rock and coal, respectively.

For the intact rock-coal combined body, its structural strength is synthetically determined by the strengths of rock and coal far away and near the bedding plane (Zhao *et al*. 2015). While, for the combined body with single joint in coal, its structural strength is also determined by the joint plane strength. Thus, the structural strength of combined body with single joint in coal can be determined by the following equation.

$$\sigma_{CRCM} = F(\sigma_r, \sigma_c, \sigma_{rb}, \sigma_{cb}, \sigma_j) \tag{1}$$

where σ_{CRCM} is the structural strength of combined body with single joint in coal; σ_r and σ_{rb} denote strengths of rocks far away and near the bedding plane, respectively; σ_c and σ_{cb} denote strengths of coals far away and near the bedding plane, respectively; σ_j presents the joint plane strength; F is the influence functions of σ_r, σ_c, σ_{rb}, σ_{cb} and σ_j on σ_{CRCM}.

In section 4, the failures of rock-coal combined bodies with single joint in coal, mainly occurred within the coal body, whereas no apparent failure was observed for rock. The structural instability failure of the combined body is mainly induced by the coal body failure. Consequently, the strength of coal body mainly determines the structural strength of combined body. Therefore, σ_c, σ_{cb}, and σ_j are main factors determining the σ_{CRCM}.. σ_c, σ_{cb} and σ_j are calculated as following.

(1) Calculation of σ_c and σ_{cb}

In Fig. 6, according to the condition of static equilibrium, relationships between the derived stresses are

$$\sigma^3_T = \sigma^2_T = \sigma^3_C = \sigma^2_C = \sigma^1_r f = \sigma^1_c f = \sigma_1 f \tag{2}$$

where f represents friction coefficient on the bedding plane and suppose that the friction coefficients are same in two horizontal directions.

Assume that the coal near the bedding plane is in the ultimate stress equilibrium state, thus σ_{cb} is confirmed by employing the Coulomb-Mohr yield criterion (Mohammadi and Tavakoli 2015)

$$\sigma_{cb} = \frac{\dfrac{2c_c\cos\phi}{1-\sin\phi}}{1-\dfrac{1+\sin\phi}{1-\sin\phi}f} \tag{3}$$

where, ϕ and c_c denote the friction angle and cohesion force of coal, respectively.

Meanwhile, the strength of coal far away the bedding plane is confirmed by the following equation

$$\sigma_c = \frac{2c_c\cos\phi}{1-\sin\phi} \tag{4}$$

Due to $0°<\phi<90°$ and $f<1$, the variation of coal strength near the bedding plane compared with that of coal far away the bedding plane is

$$\Delta\sigma_c = \sigma_{cb} - \sigma_c > 0 \tag{5}$$

In Eq. (5), the coal strength near the bedding plane is larger than that of coal far away the bedding plane, implying that strength of coal near the bedding plane is enhanced, and the changed quantity of strength is directly related to friction angle and cohesion force of coal and friction coefficient on the bedding plane. Consequently, σ_c and σ_j are the main factors determining σ_{CRCM}.

(2) Calculation of σ_j

The joint in this study can be taken as a special closed crack. Therefore, based on the sliding crack model, τ and σ are confirmed by the theory of variational principles in elasticity (Zhu *et al.* 2014)

$$\begin{cases} \tau = \dfrac{\sigma_1 \sin 2\alpha}{2} \\ \sigma = \sigma_1 \sin^2\alpha \end{cases} \tag{6}$$

Considering the friction effect on the joint plane, the effective shear stress of τ_e is

$$\tau_e = \frac{\sigma_1 \sin 2\alpha}{2} - f_j \sigma_1 \sin^2\alpha \tag{7}$$

where f_j represents friction coefficient on the joint plane.

Stress intensity factor is an important parameter of linear elastic fracture mechanics, characterizing the strength and deformation of the crack tip. And it is a measure of crack propagation tendency or crack growth driving force. The effective shear stress of τ_e can cause the joint plane to produce a relative sliding, thus the joint in this study are similar to a special pure type II crack. And its stress intensity factor of K_I is 0. And stress intensity factor K_{II} is

$$K_{II} = \tau_e \sqrt{\pi \frac{L}{2}} \tag{8}$$

According to Eq. (7), Eq. (8) can be changed as

$$K_{II} = \left(\frac{\sigma_1 \sin 2\alpha}{2} - f_j \sigma_1 \sin^2\alpha \right) \sqrt{\pi \frac{L}{2}} \tag{9}$$

When the joint plane occurs relatively sliding, K_{II} satisfies the following equation.

$$K_{II} = K_{IIC} \tag{10}$$

where K_{IIC} represents fracture toughness and is material properties.

The joint plane strength of σ_j can be determined by solving the resulting equations of Eqs. (9) and (10) simultaneously (Zhu *et al*. 2014)

$$\sigma_j = \sigma_1 = \frac{2K_{IIC}}{\left[\sin 2\alpha - f_j(1-\cos 2\alpha)\right]\sqrt{\pi \dfrac{L}{2}}} \tag{11}$$

In Eq. (11), when L is a definite value, the α corresponding to the minimum joint plane strength of σ_{jmin} is called as an optimal fracture angle, which is confirmed by the following equation

$$\begin{cases} \dfrac{\partial \sigma_j}{\partial \alpha} = 0 \\ \dfrac{\partial^2 \sigma_j}{\partial \alpha^2} > 0 \end{cases} \tag{12}$$

The optimal fracture angle of α_m is determined by solving the resulting equations of Eqs. (11) and (12) simultaneously,

$$\alpha_m = \frac{1}{2}\arctan\frac{1}{f_j} \tag{13}$$

In this study, f_j=0.1, thus, α_m =42.145°. Therefore, when α is 45° close to α_m, the joint plane firstly occurs fracture, and the main failure plane is basically along the joint plane direction, as shown in Fig. 9. Now, σ_{CRCM} is mainly determined by σ_j. Thus, σ_{CRCM} is relatively small. And in Eq. (11), with the increase of L, σ_j also nonlinearly decreases. And then σ_{CRCM} decreases.

In Eq. (12), when α=0°, $\sigma_j \to \infty$, implying that the joint plane strength is infinite. Thus, the joint plane will not fracture under compressive stress. Now, σ_{CRCM} is mainly determined by σ_c. Consequently, the deterioration effect of α and L are tiny and negligible. And now, σ_{CRCM} is relatively large.

When α=90°, σ_j<0, implying that when the rock-coal combined body occurs sliding failure along the joint plane direction and the rock-coal combined body are in the tension stress state. Consequently, in a state of compression, it will not occur sliding failure along the joint plane but cutting across the coal body, as shown in Fig. 9. Now, σ_{CRCM} is mainly determined by σ_c. Meanwhile, the deterioration effects of α and L are tiny and negligible. Thus σ_{CRCM} is relatively large.

When α is 30° or 60°, the rock-coal combined body occurs a shear failure along partial joint plane direction and partially cutting across the coal body, as shown in Fig. 9. σ_{CRCM} is collectively determined by σ_j and σ_c. The strength at α of 30° or 60° is larger than that at α of 45°, but less than that at α of 0° or 90°. Additionally, in Fig. 10, with the increase of L, the length of shear failure crack along the joint plane increases. Thus the effect of σ_j on σ_{CRCM} increases. Meanwhile, in Eq. (11), with the increase of L, σ_j decreases. Thus, σ_{CRCM} also decreases. Similarly, when L is definite, with the increase of α, the σ_{CRCM} firstly decreases and then increases, presenting "V-shaped" curves. The strength is lowest at α of 45°.

However, with the increase of L, the boundary effects from the sample edges and interface on the joint become large, which affects the strength and failure characteristics of the rock-coal combined body at a certain extent, especially the failure characteristics. This analytical model could not be used for the combined body with single joint of much greater length in coal. The failure characteristics of rock-coal combined body with single joint in coal were analyzed as following.

4. Failure characteristics of the rock-coal combined body with single joint in coal

4.1 Macroscopic failure mode of rock-coal combined body with single joint in coal

The propagation and coalescence of micro-cracks forms the main control failure crack, causing structural instability failure of the rock-coal combined body (Yin *et al*. 2018, Zhao *et al*. 2016). Figs. 7 and 8 illustrates the distributions of micro-cracks in single rock sample, single coal sample, intcat rock-coal combined body and combined bodies with single joint in coal, respectively. Among tehm, the micro-cracks of single coal sample, intcat rock-coal combined body and combined bodies with single joint in coal are represented in black lines and the micro-cracks of single rock sample shown as red lines.

In Fig. 7, the single coal sample mainly occurs the shear failure and single coal sample occurs the hybrid failure, inculding the tensile failure and shear failure. And the intact combined body were destoryed by the "V" type shear failure occurred in the coal body. And no apparent damage is observed for the rock. This phenomenon can also be found in the combined body with single joint in coal. In Fig. 8, the failure of combined bodies with single joint in coal mainly occurs within the coal body. There are two main reasons for this: 1) the strength of rock is much larger than that of coal; 2) in this study, the contact surface of the combined body is bedding plane without a cohesive force, which means the rock and coal are freely superimposed into a whole body. Under this condition, the contact surface will restrict the crack propagation in coal (Yin *et al.* 2011).

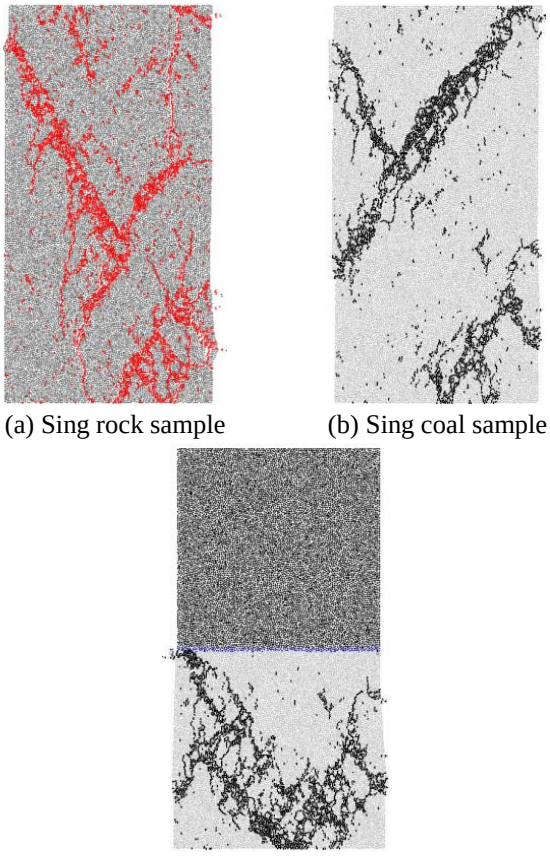

(a) Sing rock sample (b) Sing coal sample

(c) Intact combined body

Fig. 7 Distributions of micro-cracks in single rock sample, single coal sample and intact combined body

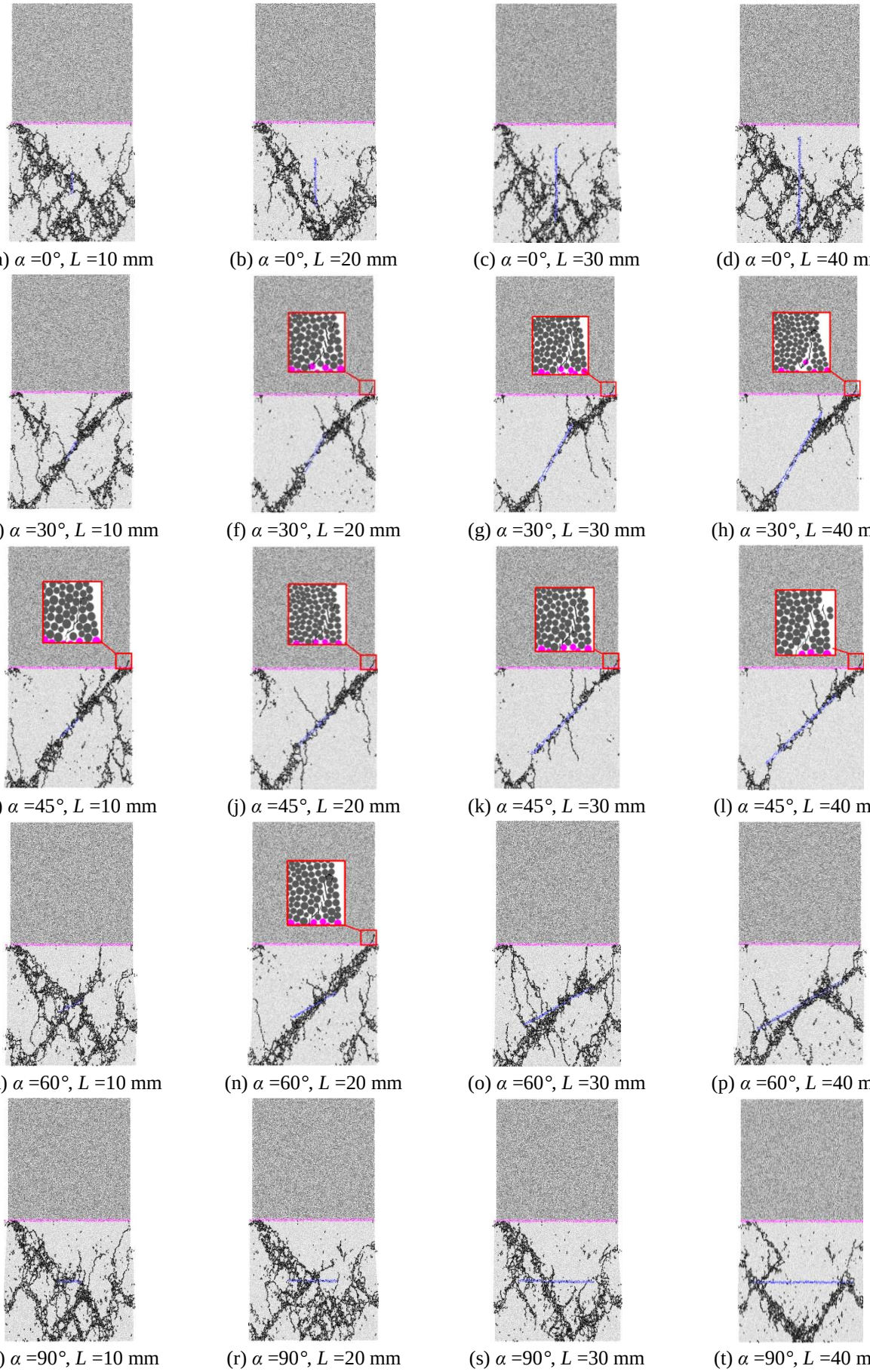

(a) α =0°, L =10 mm (b) α =0°, L =20 mm (c) α =0°, L =30 mm (d) α =0°, L =40 mm

(e) α =30°, L =10 mm (f) α =30°, L =20 mm (g) α =30°, L =30 mm (h) α =30°, L =40 mm

(i) α =45°, L =10 mm (j) α =45°, L =20 mm (k) α =45°, L =30 mm (l) α =45°, L =40 mm

(m) α =60°, L =10 mm (n) α =60°, L =20 mm (o) α =60°, L =30 mm (p) α =60°, L =40 mm

(q) α =90°, L =10 mm (r) α =90°, L =20 mm (s) α =90°, L =30 mm (t) α =90°, L =40 mm

Fig. 8 Distributions of micro-cracks in combined bodies with single joint in coal

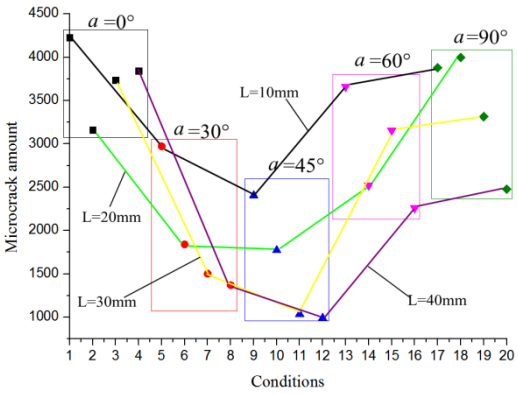

Fig. 9 Micro-crack amount of the rock-coal combined bodies under different simulation test conditions

Therefore, the rock may be not destroyed. Correspondingly, the failure of coal body mainly causes the structural instability failure of combined body. However, when α is 45° or α is 30° and L is between 20 mm and 40 mm, or α is 60° and L is 20 mm, the rock near the bedding plane is destroyed by the crack propagation in coal, as shown in a red line box of Fig. 8. This is because that the strength of rock near the bedding plane is weakened by the frictional restraint stress caused by the differences in the elastic moduli and Poisson ratios of rock and coal (Yin *et al.* 2018).

When α is 0° or 90°, the combined body mainly occurs shear failure with multiple failure planes cutting across the coal body, accompanied by some axial tensile cracks. The main control failure cracks approximately present a V-shaped failure, which is basically consistent with that of intact combined body. And the coal body is more broken due to the propagation and coalescence of the failure planes, verified in Fig. 9. Fig. 9 shows the micro-crack amounts under different simulation test conditions. In Fig. 9, the micro-crack amounts at α of 0° and 90° are larger than that of other simulation test conditions. When α is 0°, the failure mode is barely affected with the increase of L. While, when α is 90°, with the increase of L, the width of the main control shear failure zone decreases and the main V-shaped control shear failure cracks are more obvious. When α is 90° and L is 40 mm, the main V-shaped control shear failure cracks are at the lower part of joint plane. And this is because that the boundary effects from the side edges become large with the increase of L.

When α is 30° or 60°, the joint in coal affects the failure mode of combined body. And they mainly occurs shear failure along partial the joint plane direction and partially cutting across the coal body, accompanied by some axial tensile cracks, which is different from that of intact combined body. With the increase of L, the length of shear failure plane along the joint plane increases. While, when α is 60° and L is 10 mm, the rock-coal combined body mainly occurs a V-shaped shear failure cutting across the coal body accompanied with shear failure around the joint plane, implying relatively small effects of L and α on the failure mode. Also,with the increase of L, the boundary effects from the sample edges are enhanced. And the coal body close the edges are more broken.

When α is 45°, the combined body occurs shear failure basically along the joint plane direction accompanied by some axial tensile cracks. With the increase of L, the distance from the lower end of joint to the bottom of coal decreases. And the boundary effects are more obvious. Therefore, the propagation direction of the shear crack at the lower joint tip occurs a deflection at a small angle to the joint plane direction.

Additionally, in Fig. 9, with the increase of α, the micro-crack amount firstly decreases and then increases under the same condition of L. The micro-crack amount at α of 45° is the smallest. While, with the increase of L, the micro-crack amount nonlinearly decreases under a same condition of α, especially at α of 30° and 45°. Meanwhile, the propagation and coalescence of the axial tensile cracks cause the fluctuations in micro-crack amount at α of 0°, 90° and 60°. But with the increase of L, their micro-crack amounts present a basical decrease trend.

4.2 Crack propagation and coalescence process of the rock-coal combined body

As a discrete element method, the major advantage of parallel bond model in PFC^{2D} software is that complex empirical constitutive behaviour can be replaced by simple particle contact logic (Zhang and Wong 2012) and they studied the cracking processes in rock-Like material containing a single flaw under uniaxial compression using PFC^{2D} software. With the introduction of the parallel bond model, Potyondy and Cundall (2004) showed how discontinuum modelling technique could be used to simulate rock behaviour, including spalling. Yang and Huang (2014) analyzed the effect of fissure angle on the strength and deformation behavior of sandstone specimens using PFC^{2D} software and laboratory test. And the results show that the PFC model can well simulate the crack propagation. Tian *et al.* (2017) conducted experiment and mumerical simulation to investigate the effect of ligament angle on tensile strength and failure mode of Brazilian disk containing non-complanar filled fissures. And the results can well agree with the experimental result. According to the failure models of the rock-coal combined body with single joint in coal, four simulation test conditions were selected for analyze the crack propagation and coalescence process, i.e., α is 0° and L is 30 mm, α is 30° and L is 30 mm, α is 45° and L is 30 mm and α is 60° and L is 10 mm. Fig. 10 gives the micro-cracks distributions of four simulation test conditions at different axial stress.

In Fig. 10, it can be seen that the crack propagation and coalescence processes of combined bodies under different simulation test conditions are different. When α is 0 ° and L is 30mm, micro-cracks are firstly randomly distributed in coal. With the increase of axial loading, micro-cracks coalesce for forming the crack nucleation on the lower right side of the coal, as shown in the red ellipse in the Fig. 10 (a). With the further increase of axial loading, the micro-cracks in the crack nucleation propagates and form a shear-tensile crack on the lower right side of the coal, as shown in the red line in the Fig. 10 (a 3). Meanwhile, more micro-cracks are generated for forming other crack nucleations. In post-peak stage, the propagation and coalescence of micro-cracks in the crack nucleations form the main failure control crack, causing the final failure of rock-coal combined body.

While, when α is 30° and L is 30 mm or α is 45° and L

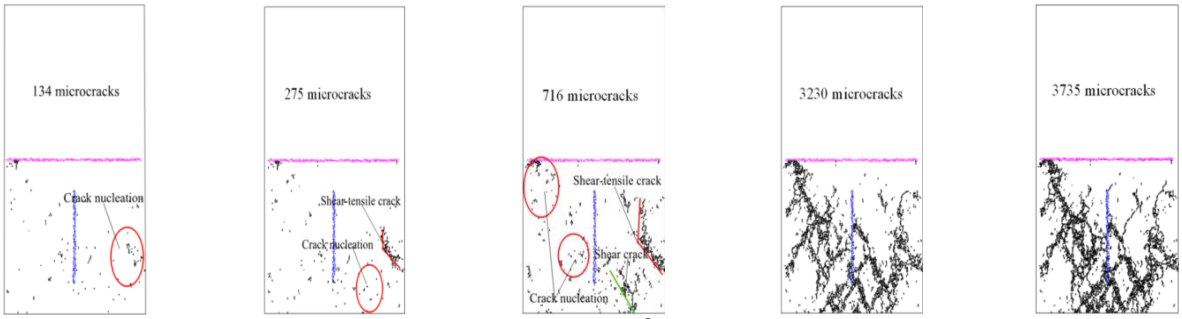

1:ε=2.99×10^{-3} σ=22.716 MPa

2:ε=3.16×10^{-3} σ=23.727 MPa

3:ε=3.41×10^{-3} σ=24.625 MPa (peak stress)

4:ε=4.24×10^{-3} σ=13.177 MPa

5:ε=5.69×10^{-3} σ=2.463 MPa

(a) α is 0° and L is 30mm

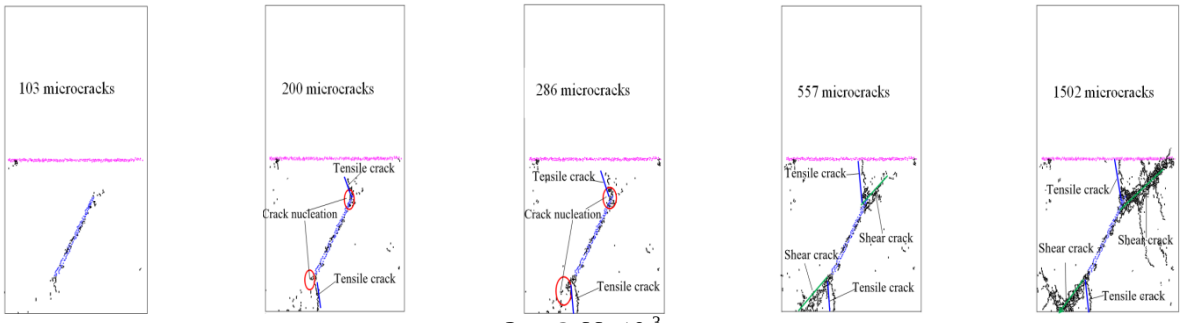

1: ε=2.28×10^{-3} σ=16.818 MPa

2: ε=2.53×10^{-3} σ=18.048 MPa

3: ε=2.66×10^{-3} σ=18.523 MPa (peak stress)

4: ε=2.89×10^{-3} σ=17.873 MPa

5: ε=4.67×10^{-3} σ=1.08 MPa

(b) α is 30° and L is 30mm

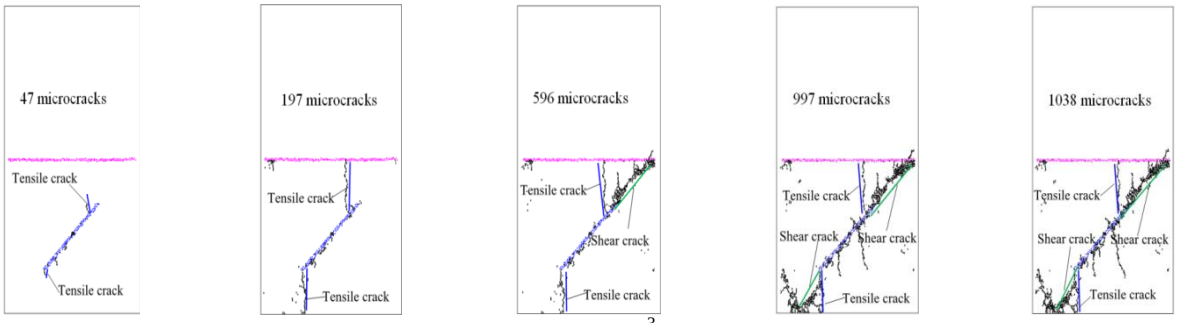

1: ε=1.61×10^{-3} σ=11.856 MPa

2: ε=2.23×10^{-3} σ=14.751 MPa

3: ε=2.75×10^{-3} σ=16.273 MPa (peak stress)

4: ε=3.17×10^{-3} σ=8.245 MPa

5: ε=3.59×10^{-3} σ=1.635 MPa

(c) α is 45° and L is 30 mm

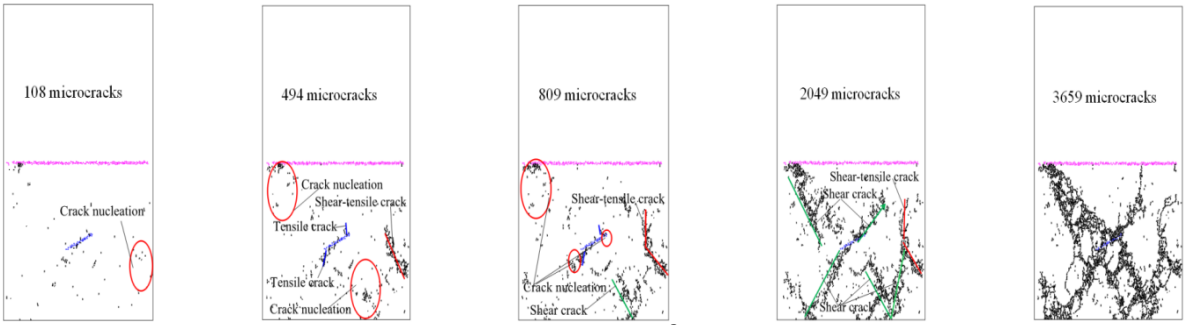

1: ε=2.84×10^{-3} σ=21.634 MPa

2: ε=3.26×10^{-3} σ=24.092 MPa

3: ε=3.424×10^{-3} σ=24.404 MPa (peak stress)

4: ε=3.76×10^{-3} σ=20.458 MPa

5: ε=6.43×10^{-3} σ=2.437 MPa

(d) α is 60° and L is 30 mm

Fig. 10 Crack propagation and coalescence process of rock-coal combined bodies

is 30 mm, micro-cracks are firstly distributed around the joint plane. With the increase of axial loading, the axial tensile cracks are generated in or close to the joint tips, as shown in the blue lines of the Fig. 10(c) and 10(d). But when the tensile cracks propagate to a certain extent, their propagations are restricted. For example, the propagation of tensile crack at α of 45° stops when they propagate to the bedding plane or the bottom of the coal. These illustrate the bedding plane restricts the crack propagation of tensile crack, and this phenomenon is basically consistent with research results studied by Yi *et al.* (2011). And micro-cracks coalesce for forming crack nucleation in or close to the joint tips, as shown in the red ellipse in the Fig. 10(c) and 10(d). With the further increase of axial loading, micro-cracks in the crack nucleation propagate to form the shear cracks, as shown in the green line of Fig. 10(c) and 10(d). And the shear cracks propagate and coalesce for forming the main failure control crack, causing the final failure of the rock-coal combined body.

Additionally, when α is 60° and L is 10 mm, micro-cracks are firstly randomly distributed in coal. With the increase of axial loading, micro-cracks coalesce for forming the crack nucleation on the lower right side or at the bottom of the coal, and the tensile cracks are generated in the joint tip, as shown in the red ellipse and blue lines of the Fig. 10 (d2), respectively. The micro-cracks in the crack nucleations propagates and form a shear-tensile crack on the lower right side of the coal and a shear crack at the bottom of the coal, as shown in the red and green lines of the Fig. 10 (d3), respectively. Meanwhile, more micro-cracks are generated for forming other the crack nucleations. And the shear cracks are generated in the coal body and the joint tips, as shown in the green lines of the Fig. 10 (d4). Finally, the V-shaped shear crack cutting across the coal body cause the final failure of the combined body.

5. Conclusions

Based on the above numerical results, the following conclusions can be drawn:

• The joint length and joint angle do not affect the compression failure process of the rock-coal combined body, but affect the strain required for each stage and have a deterioration effect on the strength of the combined body, and affect its failure modes.

• When α is 0° or 90°, the deterioration effect of L on the strength can be neglected. With the increase of L, the peak stress and peak strain occur a tiny change. While, when α is between 30° and 60°, the deterioration effect of L on the strength are relatively large. With the increase of L, the peak stress and peak strain decrease. Additionally, the deterioration effect of α on the strength becomes larger with the increase of L. With the increase of α, the peak stress and peak strain firstly decrease and then increase, presenting a "V-shaped" curve. The peak stress and peak strain at α of 45° are lowest under a same condition of L.

• The failure of the rock-coal combined body mainly occurs within coal and no apparent failure is observed for rock. Three typical typical failure modes are found for the rock-coal combined body with single joint in coal i.e., V-shaped shear failure cutting across the coal body, shear failure along partial the joint plane direction and partially cutting across the coal body and shear failure along the joint plane direction. V-shaped shear failure cutting across the coal body mainly occurs at α of 0° or 90°, while shear failure along partial the joint plane direction and partially cutting across the coal body occurs at α of 30°, 45° and 60°. However, when α is 60° and L is 10 mm, the combined body mainly occurs a V-shaped shear failure cutting across the coal body, implying relatively small effects of L and α on the failure characteristics.

• When α is between 30° and 60° (except when α is 60 ° and L is 10 mm), tensile cracks are firstly generated in or close to the joint tip. But when propagating to a certain extent, their propagations will be restricted. Then secondary shear cracks are generated in or close to the joint tip. And the propagation and coalescence of secondary shear cracks cause the structural instability failure of the rock-coal combined body. While, when α is 0° or 90°, the generation of crack nucleation is random in the coal. And the coal body is more broken due to the propagation and coalescence of the multiple failure planes.

Acknowledgments

The research described in this paper was financially supported by National Natural Science Foundation of China (51474134, 51774194), Shandong Provincial Natural Science Fundation for Distinguished Young Scholars (JQ201612), Taishan Scholar Talent Team Support Plan for Advantaged & Unique Discipline Areas, Graduate student science and technology innovation project of Shandong University of Science and Technology (SDKDYC180201), Natural Science Foundation of Shandong Province (ZR2016EEB23) and Science and Technology Program of Shandong Provience University (J15LH02).

References

Cao, R.H., Cao, P., Lin, H., Pu, C.Z. and Ou, K. (2016), "Mechanical behavior of brittle rock-like specimens with pre-existing fissures under uniaxial loading, experimental studies and particle mechanics approach", *Rock Mech. Rock Eng.*, **49**(3), 763-783.

Chen, S.J., Yin, D.W., Cao, F.W., Liu, Y. and Ren, K.Q. (2016), "An overview of integrated surface subsidence-reducing technology in mining areas of China", *Nat. Hazards*, **81**(2), 1129-1145.

Chen, S.J., Yin, D.W., Zhang, B.L., Ma, H.F. and Liu, X.Q. (2017), "Study on mechanical characteristics and progressive failure mechanism of roof-coal pillar structure body", *Chin. J. Rock Mech. Eng.*, **36**(7), 1588-1598 (in Chinese).

Huang, B.X. and Liu J.W. (2013), "The effect of loading rate on the behavior of samples composed of coal and rock", *J. Rock Mech. Min. Sci.*, **61**, 23-30.

Landriani, G.S. and Taliercio, A. (1987), "A note on failure conditions for layered materials", *Meccanica*, **22**(2), 97-102.

Liang, Z.Z., Xing, H., Wang, S.Y., Williams, D.J. and Tang, C.A. (2012), "A three-dimensional numerical investigation of the fracture of rock specimens containing a pre-existing surface flaw", *Comput. Geotech.*, **45**(9), 19-33.

Liu, J., Wang, E.Y., Song, D.Z., Wang, S.H. and Niu, Y. (2015), "Effect of rock strength on failure mode and mechanical behavior of composite samples", *Arab. J. Geosci.*, **8**(7), 4527-4539.

Lee, H. and Jeon, S. (2011), "An experimental and numerical study of fracture coalescence in pre-cracked specimens under uniaxial compression", *J. Solids Struct.*, **48**(6), 979-999.

Lu, C.P., Liu, G.J., Liu, Y., Zhang, N., Xue, J.H. and Zhang, L. (2015), "Microseismic multi-parameter characteristics of rockburst hazards induced by hard roof fall and high sress concentration", *J. Rock Mech. Min. Sci.*, **76**, 18-32.

Manouchehrian, A., Sharifzadeh, M., Marji, M.F. and Gholamnejad, J. (2014), "A bonded particle model for analysis of the flaw orientation effect on crack propagation mechanism in brittle materials under compression", *Arch. Civ. Mech. Eng.*, **14**(1), 40-52.

Mishra, B. and Verma, P. (2015), "Uniaxial and triaxial single and multistage creep tests on coal-measure shale rocks", *J. Coal Geol.*, **137**, 55-65

Mohammadi, M. and Tavakoli, H. (2015), "Comparing the generalized Hoek-Brown and Mohr-Coulomb failure criteria for stress analysis on the rocks failure plane", *Geomech. Eng.*, **9**(1), 115-124.

Kulatilake, P., Malama, B. and Wang, J. (2001), "Physical and particle flow modeling of jointed rock block behavior under uniaxial loading", *J. Rock Mech. Min. Sci.*, **38**(5), 641-657.

Park, J.W. and Song, J.J. (2009), "Numerical simulation of a direct shear test on a rock joint using a bonded-particle model", *J. Rock Mech. Min. Sci.*, **46**(8), 1315-1328.

Petukhov, I.M. and Linkov, A.M. (1979), "The theory of post-failure deformations and the problem of stability in rock mechanics", *J. Rock Mech. Min. Sci. Geomech. Abstr.*, **16**(2), 57-76.

Potyondy, D.O. and Cundall, P.A. (2004), "A bonded-particle model for rock", *J. Rock Mech. Min. Sci.*, **41**(8), 1329-1364.

Tian, W.L., Yang, S.Q. and Huang, Y.H. (2017), "An experiment and particle flow study of Brazilian disk containing two non-coplanar filled fissures", *J. China Univ. Min. Technol.*, **46**(3), 537-545 (in Chinese).

Yang, S.Q. (2015), "An experimental study on fracture coalescence characteristics of brittle sandstone specimens combined various flaws", *Geomech. Eng.*, **8**(4), 541-557.

Yang, S.Q. and Huang, Y.H. (2014), "Experiment and particle flow simulation on crack coalescence behavior of sandstone specimens containing double holes and a single fissure", *J. Basic Sci. Eng.*, **22**(3), 584-597 (in Chinese).

Yi, C., Zhu, H.G., Wang, H.T., Liu, Z. and Pan, H. (2011), "Analysis of transformation conditions and influence factors of uni-body and bi-body models under axial compression", *Rock Soil Mech.*, **32**(5), 1297-1376 (in Chinese).

Yin, D.W., Chen, S.J., Liu, X.Q. and Ma, H.F. (2018), "Effect of joint angle in coal on failure mechanical behavior of rock-coal combined body", *Quart. J. Eng. Geol. Hydrogeol.*, **51**(2), 202-209.

Zhang, Z.P. and Wong, L.N.Y. (2012), "Cracking processes in rock-like material containing a single flaw under uniaxial compression: A numerical study based on parallel bonded-particle model approach", *Rock Mech. Rock Eng.*, **45**(5), 711-737.

Zhao, T.B., Guo, W.Y., Lu, C.P. and Zhao, G.M. (2016), "Failure characteristics of combined coal-rock with different interfacial angles", *Geomech. Eng.*, **11**(3), 345-359.

Zhao, Z.H., Wang, W.M., Dai, C.Q. and Yan, J.X. (2014), "Failure characteristics of three-body model composed of rock and coal with different strength and stiffness", *Trans. Nonferr. Metal. Soc. Chin.*, **24**(5), 1538-1546.

Zhao, W.H., Huang, R.Q. and Yan, M. (2015), "Mechanical and fracture behavior of rock mass with parallel concentrated joints with different dip angle and number based on PFC simulation", *Geomech. Eng.*, **8**(6), 757-767.

Zhu, C.Q., Ma, X.F., Zhang, X.F. and Guo, F. (2014), "Effect of single closed crack on coal and rock mass fracture behavior under uniaxial compression", *Safety Coal Mines*, **10**, 169-172 (in Chinese).

Zuo, J.P., Xie, H.P., Meng, B.B. and Liu, J.F. (2011), "Experimental research on loading-unloading behavior of coal-rock combination bodies at different stress levels", *Rock Soil Mech.*, **32**(5), 1287-1296 (in Chinese).

JS